Technical paper

Ex-situ characterisation of gas diffusion layers for proton exchange membrane fuel cells

Ahmad El-kharouf [a], Thomas J. Mason [b], Dan J.L. Brett [b], Bruno G. Pollet [c,*]

[a] PEM Fuel Cell Research Group, Centre for Hydrogen and Fuel Cell Research, School of Chemical Engineering, The University of Birmingham, Edgbaston, Birmingham B15 2TT, UK
[b] Centre for CO_2 Technology, Department of Chemical Engineering, University College London, London WC1E 7JE, UK
[c] HySA Systems Competence Centre, SAIAMC, Faculty of Sciences, University of the Western Cape, Private Bag X17, Bellville 7535, South Africa

HIGHLIGHTS

► This study focuses on generating important *ex-situ* GDL parameters.
► The paper highlights the various types of commercial GDLs and discusses their characteristic variations.
► The paper shows the relationship between several *ex-situ* GDL parameters.
► The study explores the effect of PTFE loading and MPL presence upon the *ex-situ* characteristics of the GDL.
► This study emphasizes the need of parameters optimisation in GDL design and fabrication.

ARTICLE INFO

ABSTRACT

This paper presents the first part of a complete *ex-situ* characterisation of a wide range of commercial Gas Diffusion Layers (GDLs) used in low temperature and high temperature Proton Exchange Membrane (PEM) fuel cells. Physical and electrical characteristics of the GDLs are reported. The results show that the substrate structure has a significant effect on the mechanical and electrical properties of the GDL. Moreover, the Micro Porous Layer (MPL) structure determines the roughness of the surface, and affects the permeability and porosity of the GDL. It was found that the substrate treatment with PTFE affects the GDL characteristics; PTFE loading increases the GDLs hydrophobicity and permeability, however, decreases its overall porosity and resistivity. Adding a MPL to the substrate, results in a decrease in porosity and permeability and an increase in resistivity. The contact resistance of the GDL and the bipolar plate increases when the GDL thickness and PTFE loading are increased. This technical paper shows a close relationship between GDL materials and their physical characteristics and highlights the importance of optimising GDLs for fuel cell applications.

© 2012 Elsevier B.V. All rights reserved.

1. Introduction

Gas Diffusion Layers (GDLs) are important sub-components in Membrane Electrode Assemblies (MEAs) used in Proton Exchange Membrane Fuel Cells (PEMFCs). The GDL with its porous nature plays an essential and important role to allow the Hydrogen Oxidation Reaction (HOR) and Oxygen Reduction Reaction (ORR) in the Catalyst Layers (CLs) (anode and cathode respectively) to occur by diffusing the reactants (hydrogen and oxygen/air) from the flow field channels (on the flow field plates) to reach the active sites on the electrocatalyst. The GDL also facilitates water (and heat) management in the MEA by allowing water vapour to diffuse into the MEA together with the reactants to ensure sufficient humidification. The GDL also facilitates the removal of the liquid water produced on the cathode side to prevent flooding and the blocking of the catalyst. The GDL is electrically connected to the CL and acts as a supporting structure for it. In addition, the GDL is an electrical conducting medium that transfers electrons between the CL and the flow field or bipolar plates (BPPs) (Fig. 1).

GDLs are made of porous electrically conductive materials, mainly carbon based. Typically for GDLs, the carbon substrates are water proofed (e.g. by adding PTFE) to prevent the blockage of pores with water that can disrupt diffusion of reactants to the CLs during fuel cell operation. A Micro Porous Layer (MPL) made of carbon and a hydrophobic agent (e.g. PTFE), is often added on the GDL surface between the CL and the GDL. This has the function of
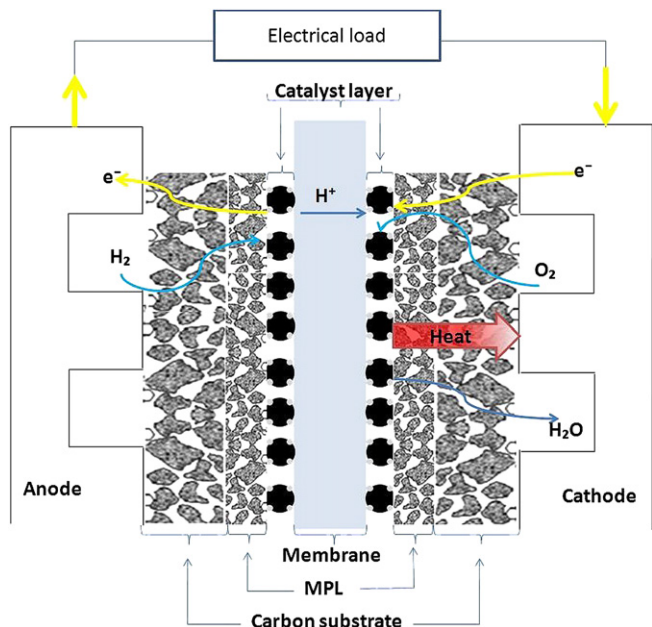
Fig. 1. GDL structure and MEA sub-components in a PEM fuel cell.

enhancing the water removal from the CL, minimising the electrical contact resistance with the adjacent CL, and preventing the catalyst ink (Pt/C/Nafion®) from penetrating through the GDL, thereby increasing the catalyst utilisation and reducing the tendency of electrode flooding [1–3]. Furthermore, it has been reported that the presence of the MPL in PEM fuel cell electrodes improves performance and enhances durability [4–6]. A description of GDL fabrication, materials, characterisation methods and degradation processes has been recently reviewed by El-kharouf and Pollet [7] and the relationship between characteristics and fuel cell performance by Cindrella et al. [8].

Studies on GDL materials include: (i) methods of ex-situ characterisation [9–11], (ii) the effect of fabrication process on GDL properties [4,12,13], (iii) comparison of GDL performance in PEM fuel cells under various operating conditions [5,14,15], and (iv) degradation using both in-situ and ex-situ testing methods [6,16–20]. Studies on mechanical properties of the GDL have mainly focussed on the effect of PEM fuel cell clamping pressure on the MEA performance [21–23]. It was found that the intrusion of GDL into the flow field channels (tenting) affect reactants flow distribution, causes pressure drop across the flow field, and decreases fuel cell performance and durability [19,24,25]. One of the main functions of the GDL is transferring reactants and by-products 'in' and 'out' of the MEA, gas transport and water permeability properties are therefore important. Commonly, gas and water permeability values are often generated by using various in-house built equipments [9,26] and the application of Darcy's law, according to Equation (1).

$$Q = \frac{-kA}{\mu}\frac{\Delta P}{L} \qquad (1)$$

where, Q is the volume flow rate of the fluid in $m^3 s^{-1}$, k is the permeability of the porous medium in m^2, A is the cross sectional area of the porous medium in m^2, μ is the viscosity of the fluid in Pa s, ΔP is the pressure difference across the porous medium in Pa, L is the distance through the medium in m.

In the literature, there are far fewer investigations of GDL properties compared to fuel cell electrocatalysis and membrane electrolytes studies; however, recently it has been shown that the

transport of electrons from the catalyst to the GDL can be elucidated by studying the contact resistances of the GDL and the CL [27] as well as the GDL and the BPP [28–31]. Furthermore, thermal conductivity and its effect on temperature distribution in PEM fuel cells have also been examined [32,33].

In this study, a range of commercial GDL samples were tested in order to produce a *technical reference* for MEA/fuel cell stack designers and modellers. Future studies will include measurements of material compositions, thermal conductivity and the permeability of water and gases. In this technical paper, it will be referred to the overall material tested as GDL, however, in the discussion; sub-layers will be referred to as the substrate for the carbon fibres layer (paper or cloth) and the Micro Porous Layer (MPL).

2. Experimental methods

2.1. Commercial GDL samples

A range of both commercial woven cloth and non-woven GDL samples were tested as shown in Table 1. The table describes the GDL materials as reported by the manufacturers' technical data sheets.

2.2. Physical properties

'Real' density (g cm^{-3}) values were measured using a helium pycnometer (Micromeritics AccuPyc II 1340). A sample of the GDL material was weighted (around 50 mg) and placed in the testing cup, and then 10 readings for the density were taken over 10 cycles of pumping and evacuating helium on the sample.

Bulk density (g cm^{-3}), porosity (%), tortuosity (*dimensionless*), pore size distribution and permeability (m^2) were measured using a mercury porosimeter (Micromeritics AutoPore IV). Here, the measured permeability corresponds to mercury permeation through the GDL with increasing pressure (MPa). Experimentally,

Table 1
Commercial GDL samples and description.

Manufacturer	Type	Description
Ballard	1071HCB	Carbon cloth
	P50	P50 is the carbon paper substrate;
	P50T	P50T is a teflonated carbon paper
	GDS1120	substrate; GDS1120 is a teflonated paper with a MPL
	P75	P75 is a carbon paper substrate;
	P75T	P75T is a teflonated carbon paper
	GDS2120	substrate; GDS 2120 is a teflonated paper with a MPL
Toray	TGP-H-030	Teflonated carbon papers of various
	TGP-H-060	thicknesses
	TGP-H-090	
	TGP-H-120	
Freudenberg	C2	Felt fibres carbon paper based on H2315
	C4	substrate with a MPL applied
	I2 C6	Felt fibres carbon paper based on
	I2 C8	H2315 I2 substrate with a MPL applied
E-TEK	LT 12001200WN	Non-woven web containing a MPL
	LT	Woven web containing a MPL
Sigracet	GDL 10 BC	3-D fibres carbon paper containing a MPL
	GDL 24 BA	A carbon paper with PTFE and
	GDL 24 BC	with/without MPL as below:
	GDL 25 BA	-BA stands for 5% PTFE loading and no MPL
	GDL 25 BC	-BC stands for 5% PTFE loading with a MPL
	GDL 34 BC	-DC stands for 20% PTFE loading with a MPL
	GDL 34 DC	
	GDL 35BA	
	GDL 35 BC	
Tenax	TCC2660	Untreated woven carbon cloths
	TCC 3250	

a 1 cm^2 GDL samples (ca. 200 mg) was placed in the porosimeter stem to undergo low and high pressure mercury intrusion testing. Mercury was then deposited/inserted gradually into the sample by increasing the pressure up to 30,000 Psi ($\sim$206 MPa) whereby the GDL sample pores were filled starting from the larger pores at low pressures and down to smaller pores at higher pressures. This method allowed the measurements and determination of total pore volume, skeletal volume, real and bulk density as well as total porosity values.

Here, the Micromeritics AutoPore IV software uses the Washburn's equation to determine the pore size distribution and the pore length of the GDL sample based on the assumption that the pores are of cylindrical geometry. Furthermore, the Katz and Thompson's equation (derived from the *percolation theory*) is used by the software to calculate the absolute permeability (k) of the GDL sample. The permeability values are then used in the expression derived by Jörgen Hager to calculate tortuosity [34]. In our experimental work, all these values were automatically calculated by the Micromeritics Instruments software as detailed and explained in the paper published by Micromeritics Instruments Corp. [34].

Scanning Electron Microscopy (SEM) was used to examine the GDL surface morphology on both sides i.e., the one facing the catalyst layer with or without a MPL, and the other one facing the BPP. Similarly, the GDL roughness (μm) of each side was measured (over three areas on the sample surface) using an interferometer (Omniscan Microxam 2).

The water contact angle ($^\circ$) of the GDL was measured using the sessile drop method [35]. In this method, the contact angle of the water droplet on the solid surface of the GDL and the MPL was measured using an image processing software developed by Teaer Coating Ltd/MIBA. Measurements were carried out by using three different droplet sizes for each sample.

2.3. Electrical properties

In-plane electrical resistance was measured using the method reported by Williams *et al.* [11]. GDL samples of 2 mm width and 100 mm length were manually cut and the resistance was measured at 10 mm increments (10 points in total). Here, the measured resistance (R) values were plotted against distances (l) and yielded a linear relationship whereby the slope of the line represented the *in-plane* resistance per unit of distance (R').

The GDL samples *in-plane* resistivity (ρ) values were calculated using Ohm's Law as shown in Equation (2):

$$R = (\rho l)/A \rightarrow \rho = (RA)/l \qquad (2)$$

where, R is the resistance of the GDL in Ω, ρ is the *in-plane* resistivity in Ω m, A is the cross-sectional area of the GDL sample in m^2 l is the length of the GDL sample in m.

The contact resistance (R_c) between a 4 cm^2 GDL and 'plane' POCO graphite (POCO AXF-5Q) plates (industry standard material often used as a *reference* material) was measured at various clamping pressures. The clamping pressure was monitored using a controlled compression device (Zwick Roel Z030). The GDLs were preconditioned by applying a pressure of 3 MPa (3 times) before conducting the test. This step was performed to eliminate the effect of 'irreversible' deformation of the GDL as (i) the contact resistance values became repeatable and (ii) the irreversible changes were found to be negligible after the 3rd compression. The GDL was placed between the two POCO graphite plates and the two gold plated stainless steel (SS) current collectors as shown in Fig. 2. The resistance was measured by the 4-wire Kelvin method using a BS407 precision Milli/Micro-Ohmmeter (resolution of 1 $\mu\Omega$ with 0.1% of resolution accuracy). The contact resistance between the POCO
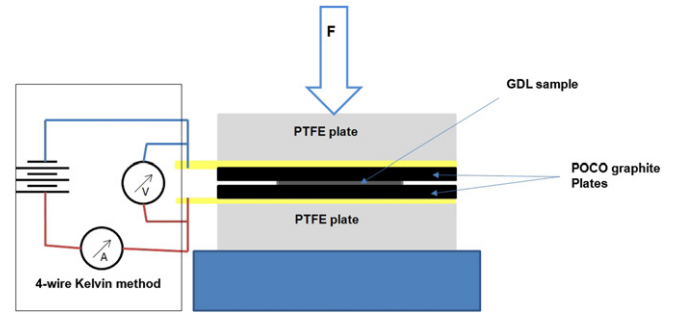

Fig. 2. Electrical contact resistance measurement setup.

plates and the gold plated SS plates was measured using a similar arrangement, where one POCO plate was placed between the two gold plated SS plates. All measured resistance values were used to calculate the contact resistances using the following equations:

$$R_{\text{measured}} = 2xR_{c,\text{SS-Au/FFP}} + 2xR_{c,\text{FFP/GDL}} + 2xR_{\text{FFP}} + R_{\text{GDL}} \qquad (3)$$

and

$$R_{\text{FFP measured}} = 2xR_{c,\text{ SS-Au/FFP}} + R_{\text{FFP}} \qquad (4)$$

where, $R_{c,\text{FFP/GDL}}$ is the contact resistance between the GDL and the POCO graphite flow field plate $R_{c,\text{SS-Au/FFP}}$ is the contact resistance between the POCO graphite flow field plate and the gold plated stainless steel plate R_{FFP} is the *through-plane* resistance of the POCO graphite flow field plate R_{GDL} is the *through-plane* resistance of the GDL.

Subtracting Equations (3) to Equation (4) gives Equation (5):

$$R_{\text{measured}} - R_{\text{FFP measured}} = 2xR_{c,\text{FFP/GDL}} + R_{\text{FFP}} + R_{\text{GDL}} \qquad (5)$$

Thus rearranging Equation (5), one obtains the contact resistance between the GDL and the POCO graphite flow field plate ($R_{c,\text{FFP/GDL}}$):

$$R_{c,\text{FFP/GDL}} = (R_{\text{measured}} - R_{\text{FFP measured}} - R_{\text{FFP}} - R_{\text{GDL}})/2 \qquad (6)$$

If it is assumed that R_{FFP} and R_{GDL} are negligible due to their low resistance values, Equation (6) may be simplified to:

$$R_{c,\text{FFP/GDL}} = (R_{\text{measured}} - R_{\text{FFP measured}})/2 \qquad (7)$$

For example, POCO graphite plates have very low resistivity ($\sim$1.470 mΩ cm) [36] and using Equation (2), the resistance of the POCO graphite plate used (area=4 cm^2, thickness=3 mm) was calculated to be 0.110 mΩ. Thus in our conditions, R_{FFP} and similarly, the GDL *through-plane* resistance ($R_{\text{GDL}} < 10^{-3} - 10^{-6}$ Ω) can be neglected under the range of clamping pressures used [37,38]. In this paper, the simplified Equation (7) is used for the determination of contact resistance between the GDL and the POCO graphite flow field plate.

3. Results and discussion

3.1. Physical properties (thickness and density)

Thickness, area weight, bulk and real (material) density are important physical parameters for GDL materials. Thickness has

Table 2
Woven GDLs weave and fibres properties.

	Weave width (μm)	Fibre diameter (μm)
1071HCB	350 − 500	8 − 9
TCC2260	200 − 250	8 − 9
TCC3250	250 − 375	11 − 12
LT1200W	450 − 500	8 − 11

Table 3
Commercial GDL properties.

Material	Manufacturer materials' properties			Measured properties											
	Thickness (μm)	Area weight (gm⁻²)	Bulk density (gcm⁻³)	Real density (gcm⁻³)	Bulk density (gcm⁻³)	Surface roughness (μm)		Porosity %	Tortuosity	Mean pore diameter (nm)	Permeability (m²)	Water contact angle, (°)	Contact resistance (mΩ cm²)		In-plane resistivity (Ω m)
						Sa	Sq				Mercury	Contact angle	@ 1.5 MPa	@ 2.5 MPa	
1071HCB	356	123	0.35	1.816 ± 0.002	0.39	–	–	64.9	1.95	3401	2.36E-11	68 ± 4	52.66	30.87	1.28E-04
P50	170	50	0.32	2.083 ± 0.004	0.36	14.7 ± 0.8	19.8 ± 0.5	48.7	3.01	993	9.21E-12	111 ± 7	2.13	1.56	2.70E-03
P50T	180	62	0.34	2.151 ± 0.004	0.37	15.7 ± 0.6	19.4 ± 0.3	44.9	2.55	1528	1.41E-11	114 ± 1	2.60	1.85	2.28E-03
GDS1120	210	79	0.40	2.125 ± 0.005	0.46	20.0 ± 3.0	25.0 ± 4.0	44.8	3.24	859	4.73E-12	116 ± 16	–	–	2.62E-03
P75	230	75	0.33	2.083 ± 0.005	0.35	14.2 ± 0.9	20.0 ± 2.0	62.4	2.43	2074	1.11E-11	107 ± 7	2.40	1.73	4.27E-03
P75T	255	88	0.33	2.087 ± 0.003	0.36	14.0 ± 1.0	18.0 ± 2.0	59.9	2.23	1227	1.31E-11	113 ± 3	2.82	1.99	2.40E-03
GDS2120	260	101	0.40	2.131 ± 0.005	0.40	17.0 ± 2.0	23.0 ± 5.0	60.2	2.62	2998	6.06E-12	85 ± 3	–	–	2.78E-03
TGP-H-030	110	–	0.40	2.071 ± 0.001	0.37	14.0 ± 1.0	18.1 ± 0.9	64.6	2.50	2625	1.07E-11	133 ± 4	2.74	1.99	9.90E-05
TGP-H-060	190	–	0.44	2.002 ± 0.003	0.43	14.1 ± 0.2	19.1 ± 0.6	63.1	2.76	2631	6.15E-12	129 ± 9	3.27	2.40	9.50E-05
TGP-H-090	280	–	0.44	2.019 ± 0.003	0.49	13.0 ± 0.5	17.9 ± 0.4	67.2	2.55	3324	4.53E-12	138 ± 8	3.64	2.77	7.28E-05
TGP-H-120	370	–	0.45	1.985 ± 0.004	0.49	12.2 ± 0.5	17.3 ± 0.8	61.8	2.51	1717	3.90E-12	120 ± 1	4.60	3.23	4.44E-05
C2	250	130		1.882 ± 0.002	0.57	14.6 ± 0.4	19.6 ± 0.9	49.2	4.51	658	9.12E-13	121 ± 4	3.00	2.23	1.45E-04
C4	250	130	–	1.900 ± 0.002	0.49	14.0 ± 1.0	18.9 ± 0.6	61.0	4.26	158	1.04E-12	1173			1.70E-04
I2 C6	250	135	–	1.867 ± 0.002	0.54	9.5 ± 0.4	12.7 ± 0.4	46.2	5.02	1148	8.57E-13	61 ± 6	3.37	2.47	9.00E-05
I2 C8	230	135	–	1.934 ± 0.002	0.62	8.4 ± 0.6	11.3 ± 0.8	47.0	4.91	682	6.25E-13	122 ± 4			1.89E-04
LT 1200N	185	75	0.41	2.053 ± 0.004	0.39	17.0 ± 2.0	22.0 ± 0.8	64.9	2.74	769	6.45E-12	90 ± 6	–	–	2.93E-04
LT1200W	275	200	0.73	1.906 ± 0.002	0.50	–	–	31.8	2.74	1055	4.98E-12	96 ± 1	–	–	1.03E-04
GDL 10 BC	420	135	–	1.945 ± 0.008	0.36	24.0 ± 2.0	31.0 ± 3.0	34.6	2.95	2919	8.04E-12	122 ± 4	–	–	1.18E-04
GDL 24 BA	190	54	–	2.140 ± 0.010	0.28	13.4 ± 0.9	17.0 ± 2.0	73.9	1.40	2208	3.67E-11	98 ± 4	2.69	1.76	1.94E-03
GDL 24 BC	235	100	–	2.010 ± 0.003	0.44	13.3 ± 0.1	18.3 ± 0.8	40.0	3.00	2450	5.09E-12	104 ± 4	–	–	2.51E-03
GDL 25 BA	190	40	–	1.941 ± 0.002	0.21	22.0 ± 4.0	31.0 ± 3.0	66.2	1.45	1705	4.54E-11	–	2.52	1.85	4.78E-03
GDL 25 BC	235	86	–	2.009 ± 0.007	0.34	23.0 ± 4.0	32.0 ± 3.0	36.5	2.92	842	5.64E-12	112 ± 12	–	–	–
GDL 34 BC	315	140	–	1.987 ± 0.001	0.41	23.9 ± 0.9	30.8 ± 0.2	47.5	2.47	2197	8.97E-12	126 ± 7	–	–	2.22E-03
GDL 34 DC	–		–	1.978 ± 0.004	0.48	25.0 ± 2.0	31.0 ± 3.0	40.8	2.62	1593	6.91E-12	134 ± 2	–	–	2.51E-03
GDL 35 BA	300	54	–	2.022 ± 0.009	0.19	32.0 ± 3.0	43.0 ± 3.0	70.5	1.33	2469	5.31E-11	123 ± 8	2.55	1.85	5.51E-03
GDL 35 BC	325	110	–	1.980 ± 0.007	0.31	36.0 ± 2.0	46.0 ± 5.0	52.6	1.94	1467	1.72E-11	118 ± 11	–	–	3.67E-03
TCC-2660	260	80	0.31	1.793 ± 0.003	0.34	–	–	66.9	1.83	2291	2.96E-11	126 ± 3	2.01	1.41	3.54E-04
TCC-3250	320	100	0.31	1.803 ± 0.002	0.36	–	–	71.0	2.32	1631	1.74E-11	79 ± 7	2.38	1.67	7.68E-05

a direct effect on gas and water permeability, diffusion and electrical conductivity. Area weight and bulk density relate to the fibre density, MPL carbon density and PTFE loading in the GDL. Table 3 lists the properties for the GDL samples used in this study, from both the manufacturers' reported values and our measured values.

The data in Table 3 show that the GDL thicknesses range between 110 and 420 μm with an independent large variation in the area weight. The 'real' density measured by the pycnometer appears to be within a narrow gap of 1.8–2.15 g cm^{-3} which falls within the region between the density of carbon fibres of 1.8–2.1 g cm^{-3} and PTFE of 2.04–2.17 g cm^{-3} [39]. However, a large variation in the bulk density can be observed which is influenced by the porosity and the density of the fibres/MPL within the GDL; the measured bulk density values of the GDLs are close to the values reported from the manufacturers, and the small deviation can be due to the heterogeneous structure of the GDLs.

3.2. Fibre structure, surface morphology and roughness

The SEM images of the surface and edge view of woven and non-woven GDLs are shown in Fig. 3. Woven GDL constitutes the carbon cloth group, and the non-woven GDL makes the carbon paper group. The non-woven group can be divided into two types according to the structural configuration of the fibres in the GDL, namely, (i) straight and (ii) felt/'spaghetti' fibres.

Only a few commercial woven cloth GDLs are available due to the relatively high cost of manufacturing compared to the non-woven paper GDLs. The main difference noticed from the SEM images in the woven cloth types is the diameter of the fibres and the weave width as shown in Table 2. The SEM image for LT1200W in Fig. 4c also shows the PTFE loading on the cloth. Here, the woven structure gives the GDLs high mechanical flexibility and compressibility.

In the straight fibre structure, the fibres create a multi-layered web of interlinked fibres forming the carbon paper. This can be observed in Fig. 5 that shows the separation of these layers after testing under compression. Some differences can be seen in the SEM images of this type (Fig. 6). Graphitised binders can be noticed in some samples [Fig. 6c,d,e,f]; for example, the carbon/PTFE binding agglomerates around the fibres linking them together and decreasing the pores diameter. SEM images for the Toray papers show clear graphitised wetted fibres [Fig. 6b]. Also, from the SEM images it appears that the fibre density differs greatly from one GDL to another. This type of GDL is usually mechanically rigid and brittle and can easily break if bended.

Felt/spaghetti fibre structures are clearly observed for all Freudenberg and some SGL GDL samples. Here, the SGL 10BC (Fig. 7) is often described as a three dimensional (3-D) fibre configuration. This type of structure gives the GDL a higher mechanical flexibility and a higher compressibility compared to other carbon paper GDLs. It is interesting to note that as with straight fibre carbon papers binders can be observed in the SGL 10BC GDL, but not in all Freudenberg GDLs. Furthermore, it can be noticed that the fibres density for Freudenberg GDLs is significantly higher.

Here, the roughnesses of the carbon paper substrates surfaces were measured using an interferometer. The mean value of heights (S_a) and root mean square of heights (S_q) on the surface are listed in Table 3. The values of S_q range between 10 and 45 μm indicating high roughnesses facing the BPP material in the PEM fuel cell (Fig. 8). Avasarala et al. observed a significant effect of the surface roughness of compositae BPP on the interfacial contact resistance with the GDL [40]. This can be related to the GDLs roughness as well as the BPP; however, to the authors' knowledge, this relationship has not been explored yet. Here, Fig. 8 clearly shows a decrease in roughness for teflonated substrates compared to unteflonated (P50T and P75T compared to P50 and P75). Moreover, it shows a slight increase in the substrates roughness when a MPL is added to the other side of the GDL. Some types of GDLs are coated on one side with a MPL and the SEM images in Fig. 9 show the scale of features observed in various types of GDL. The GDS 2120 image shows a very rough surface and coarse pore sizes compared to other types, while the E-TEK media exhibit a very smooth and fine pore sizes. It can also be seen that the MPL surfaces have a sporadic distribution of pore sizes.

The roughness of the surface of the MPLs was measured using an interferometer and the values are shown in Table 4. The roughness values of the MPL in GDS1120 and GDS 2120 were found to be 8–10 times higher than the MPL in other GDL samples (Fig. 10). Cracks are observed on the MPL surfaces and even larger cracks are obtained on woven GDL containing MPL following the pattern of the weaves (Fig. 8). This observation may be due to the rough structure of the woven structure and the GDL bending caused by its high flexibility.
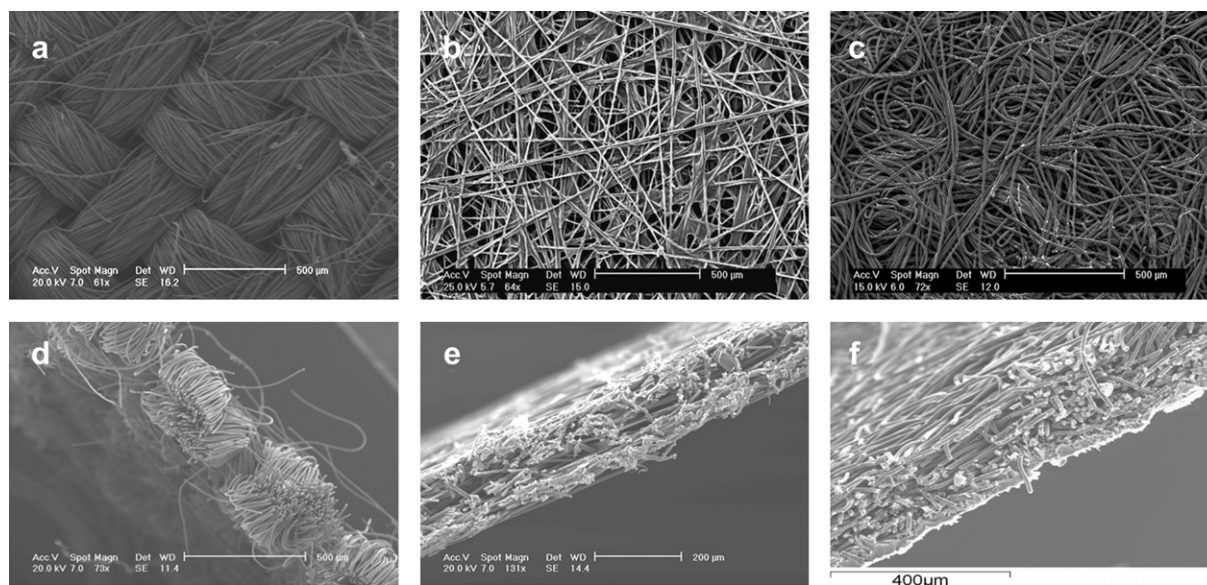

Fig. 3. SEM images of GDL fibres configuration; surface and edge views of (a) & (d) woven fibres in carbon cloth − Ballard 1071HCB, (b) and (e) straight stretched fibres in carbon paper − Toray H-060, (c)& (f) felt/spaghetti fibres in carbon paper-Freudenberg C2.
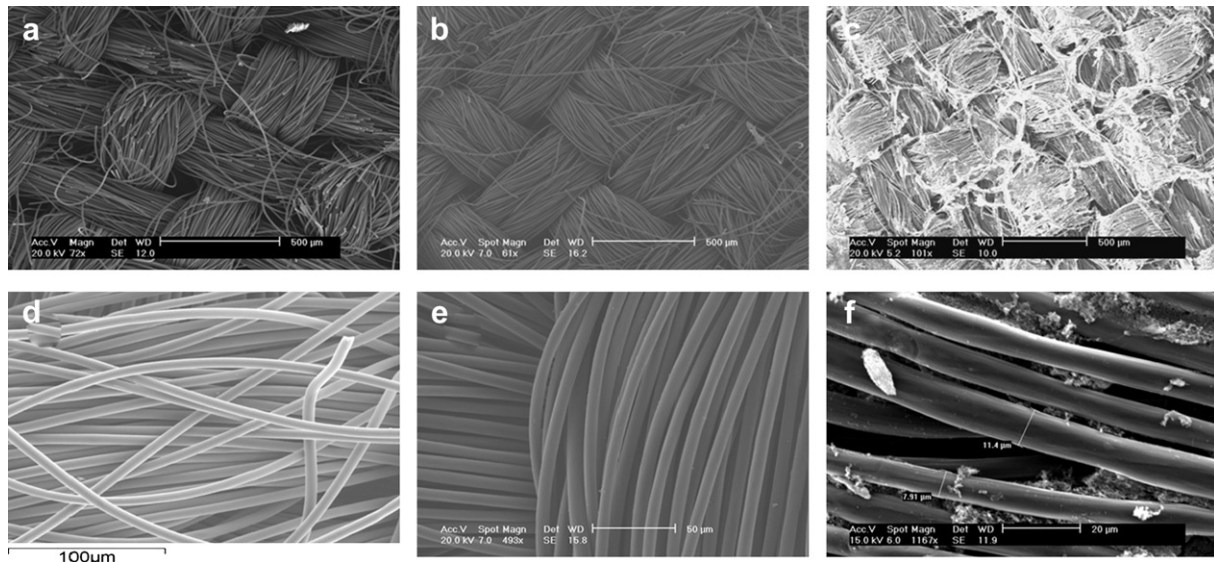
Fig. 4. SEM images of several types of woven carbon cloth sample; surface views of: (a) Tenax (b) Ballard 1071HCB, and (c) E-TEK 1200W and closer views of (d) Tenax, (e) Ballard 1071HCB, and (f) E-TEK 1200W.

The low values of the surface roughness show that the MPL creates a smoother surface for applying the catalyst ink for the fabrication of Gas Diffusion Electrodes (GDEs), in turn reducing contact resistance between the GDE and the polymeric electrolyte membrane (PEM).

3.3. Porosity, tortuosity and pore size distribution

Porosity, tortuosity and pore size distribution are important factors in determining gas and water transport through/in the GDL. The effective diffusion coefficient (D_e) can be calculated using the measured values, which is an important parameter of the GDL properties. Furthermore, the distribution and variation in pore sizes shown by the pore size distribution are important for their effect on the capillary pressure driving the water out of the PEM fuel cell [41].

Fig. 11 and Fig. 12 show the wide variation in commercial GDL porosity and tortuosity values. Porosity, tortuosity and average pore diameter values are listed in Table 3. The table clearly shows that porosity and tortuosity are affected by the presence of PTFE and

Fig. 5. Straight fibres GDL's layer separation after compression in Toray H-120.

MPL. Generally speaking, PTFE loading decreases the porosity and tortuosity. The decrease in porosity is mainly due to the blockage and narrowing of the pores and the decrease in tortuosity might be due to the blockage of closed and longer pores leaving shorter open pores for permeability. Adding a MPL introduces an extra layer with lower porosity and smaller pores resulting in a decrease in the overall porosity and thus an increase in tortuosity.

Pore size distribution measurement is commonly determined by the coverage of the volume of mercury intrusion over the range of pore diameters in the GDL material. Table 3 also shows that the average pore diameter decreases with increasing thickness; however, the bulk porosity seems to be unaffected (Fig. 11). The pore size distribution curve for the Toray samples show larger pores in TGP-H-030 and TGP-H-060 with lower volume intrusion for the latter one. TGP-H-090 and TGP-H-120 samples show a shift to smaller pore diameters. This observation of high volume intrusion and pore size in TGP-H-030 is interesting and could be due to the very small thickness of the GDL (Fig. 13). Here, the porosity values for the Toray samples are in very good agreement with those obtained by Fishman et al. [42].

However, applying a MPL on the substrate changes the pore distribution as shown in Fig. 14. The figure shows that the curve peak shifts to lower pore size values with less volume intrusion causing a significant decrease in the bulk porosity (Table 3). Fig. 15 shows the gradual change in the pore size distribution for the substrate when loaded with PTFE and a MPL. A significant decrease in the intrusion volume can be observed when the GDL is loaded with PTFE; this is also manifested in the decrease in the bulk porosity. However, when the MPL is applied, the GDL maintains constant bulk porosity. P50, P50T and GDS1120 also exhibit a similar behaviour. This finding is very interesting and could be due to the structure of the MPL as shown in Fig. 8e and the surface roughness of the MPL in these GDLs (Table 4). Furthermore, it was found that a decrease in the pore diameters was observed with increasing PTFE loading from 5% to 20% (Fig. 16) with subsequent decrease in porosity values.

Woven carbon cloths pore size distribution curves show a different trend to that of the GDL papers (Fig. 17). Volume intrusion can be observed on wide base of pore diameters that extends to high pore sizes. The results show that the three woven GDLs with no MPL
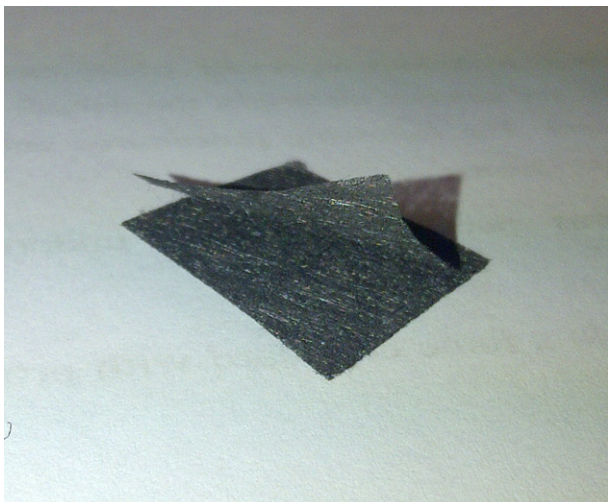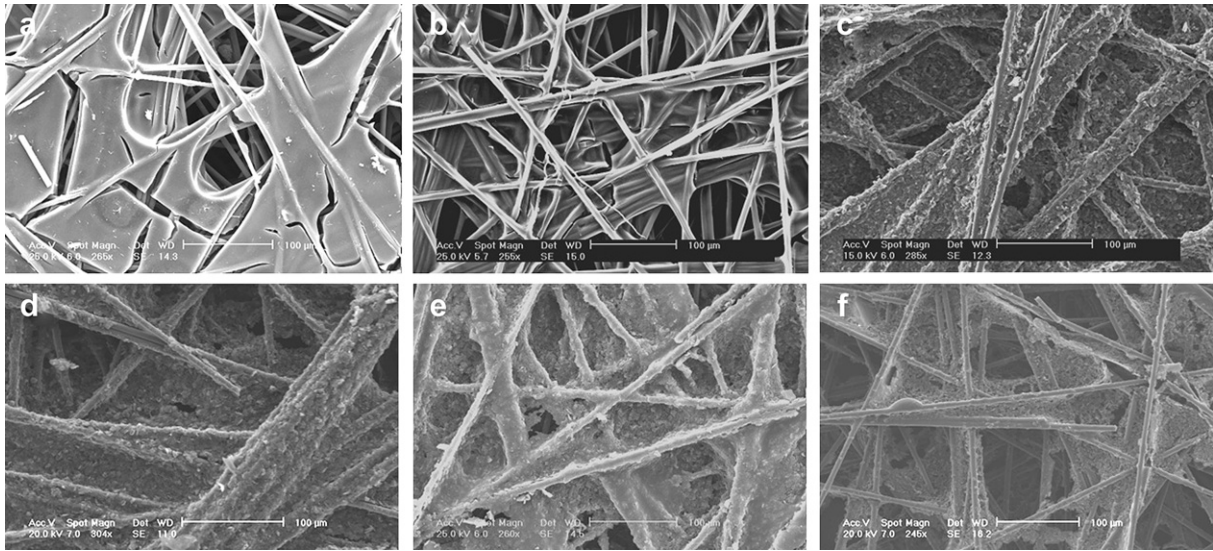
Fig. 6. SEM images of various types of straight fibres carbon paper samples: (a) Toray H-060, (b) E-TEK 1200N, (c) Ballard P75, (d) Ballard P75T; (e) AvCarb 1120; (f) Sigracet 25BA.
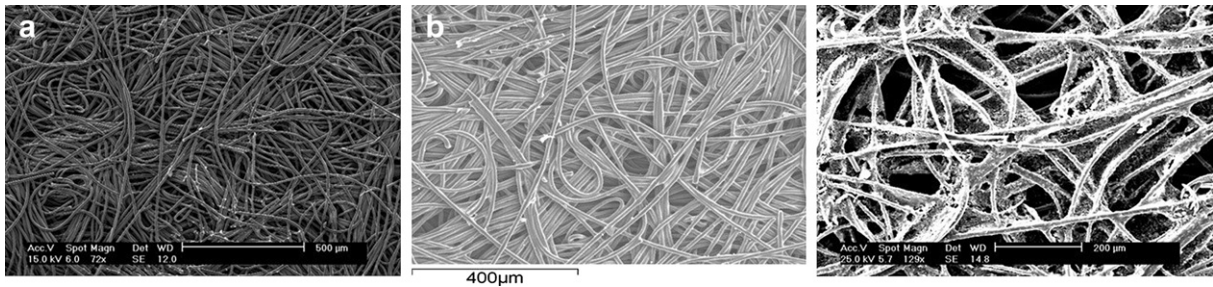

Fig. 7. A series of SEM images of felt/spaghetti fibres carbon paper samples of: (a) Freudenberg C2, (b) Freudenberg C6 and (c) SGL 10BC.

have the same bulk porosity. However, in the case of the presence of MPL in LT1200W, the curve follows the same trend but with lower intrusion volume. Furthermore, an additional sharp high peak at low pore diameter is observed which is not present in the case of carbon

papers. The volume intrusion peak at low pore diameter presents the pores in the MPL of the GDL. Again, the bulk porosity of this GDL is significantly lower than the other woven types.

3.4. Permeability

In our study, GDL permeability was measured using the mercury intrusion method at various clamping pressures. Therefore, the values reported here correspond to both *through-plane* and *in-plane* permeability of the GDL. These values show that the presence of MPL, the fibre density, thickness and PTFE loading, affect the permeability of the GDL as shown in Fig. 18. The addition of the MPL results in a decrease in the permeability of the GDL. Furthermore, it can be observed that the Freudenberg samples have low permeability compared to all other GDL samples due to the high fibre density in the GDL structure. It is interesting to note that (i) the permeability of the P50 and P75 increase with PTFE loading in P50 and P50T, which may be due to the decrease in tortuosity, and (ii) Toray papers permeability decrease with increasing thickness. Unexpectedly, woven GDLs show relatively lower permeability compared to some paper type GDLs.

3.5. Water contact angle (hydrophobicity)

The hydrophobicity and hydrophilicity of a substrate is a material and surface structure related property; the two parameters describe the strength or weakness of the bonds created between the substrate and the water molecules in contact. They determine

Fig. 8. MPLs on various commercial GDLs at two image scales: (a) & (e) GDS 2120, (b) & (f) Freudenberg C2, (c) & (g) LT1200W and (d) & (h) SGL 24BC.

Fig. 9. Surface roughness for carbon paper GDL substrates.

the behaviour of water within the GDL and the ease of its transport through it. Hence, the GDL has an important role in water management and liquid water removal from the MEA. Contact angle measurement is a powerful diagnostic for understanding the interaction of GDL material with water.

In our experiments, both hydrophobic (water contact angle > 90°) and hydrophilic (water contact angle < 90°) GDL surfaces were observed (Fig. 19), with a majority of them being hydrophobic. For most commercial GDLs, the MPL shows higher water angle (more hydrophobic) than that of the substrate. However, an interesting feature for the Sigracet GDLs is that the MPL has a lower water contact angle (less hydrophobic) than the substrate itself (Fig. 19).

It is important to note that the surface water contact angle depends upon both the hydrophobicity of the material and the roughness of the surface. Therefore, the increase in hydrophobicity on the substrate side could be due to its high roughness. The values of water contact angle for both the substrates and the MPLs are listed in Tables 2 and 3 respectively. The values reported here are within the values range reported for the various samples in the literature [43,44].

3.6. Electrical conductivity and contact resistance

The contact resistance between the GDL and the BPP varies with (i) the flow field plate material, (ii) the GDL material, (iii) the flow

Fig. 10. Surface roughness for MPLs.

field design (ratio of 'lands' to 'grooves') and (iv) the clamping pressure. The change in resistances with clamping pressures is shown in Fig. 20. The figure shows samples of straight fibre and felt fibres papers and woven fibre cloths. It is important to mention that
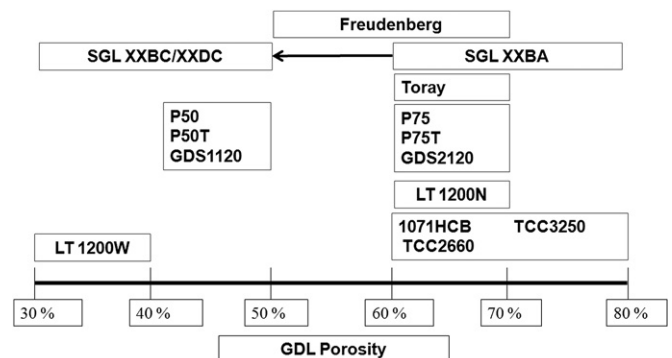
Table 4
MPL properties.

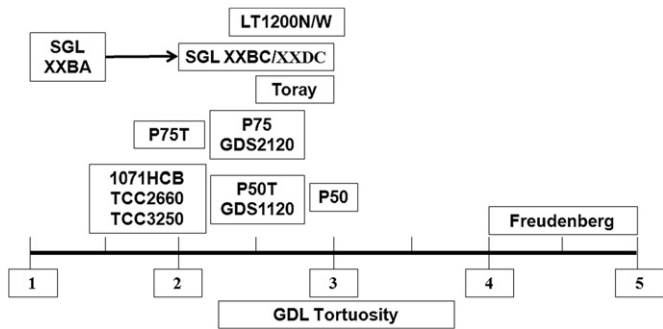|	Roughness (μm)		Water contact angle, θ (°)
	S_a	S_q	
GDS1120	9.0 ± 2.0	11.0 ± 2.0	122 ± 5
GDS2120	7.9 ± 0.6	9.5 ± 0.8	104 ± 8
C2	1.0 ± 0.1	1.3 ± 0.1	120 ± 16
C4	1.4 ± 0.3	1.8 ± 0.5	122 ± 4
C6	1.7 ± 0.2	2.3 ± 0.4	84 ± 5
C8	0.5 ± 0.1	0.6 ± 0.1	132 ± 13
LT 1200N	1.1 ± 0.2	1.5 ± 0.3	112 ± 18
LT1200W	0.5 ± 0.1	0.8 ± 0.2	129 ± 14
SGL 10BC	0.4 ± 0.1	0.5 ± 0.1	121 ± 5
SGL 24BC	1.7 ± 0.1	2.5 ± 0.3	94 ± 3
SGL 25BC	0.8 ± 0.2	1.3 ± 0.3	–
SGL 34BC	0.8 ± 0.2	1.1 ± 0.3	89 ± 5
SGL 34DC	1.5 ± 0.2	2.2 ± 0.3	93 ± 7
SGL 35BC	1.5 ± 0.4	2.2 ± 0.7	99 ± 3

Fig. 11. Porosity of commercial GDLs.

Fig. 12. Tortuosity of commercial GDLs.

compression has a partially irreversible effect on the GDL due to deformation. This can be seen when measuring the contact resistance of samples at the pre-conditioning stage. The contact resistance decreases with each compression until it reaches stabilisation, usually after 3–5 compression cycles [19].

Fig. 21 shows the GDL contact resistance at 1.5 and 2.5 MPa (clamping pressures reported in the literature) [23]. The figure shows that the contact resistances of P50/P75 and P50T/P75T increase when the samples contain PTFE in the substrate. Furthermore, the Toray GDLs show an increase in contact resistance

Fig. 13. Pore size distribution change with GDL thickness in Toray samples − (a) full pore size distribution & (b) 'zoom in' on the low pore sizes region.

Fig. 14. Pore size distribution change when a MPL is added for the samples: (a) SGL 25BA and SGL 25BC and (b) SGL 35 BA and SGL 35BC.

with a thickness increase, agreeing with the increase noticed between P50 and P75. This effect of resistance increase with thickness may be due to the increase in the *through-plane* resistance of the GDL with thickness. The woven cloth 1071HCB has significantly high contact resistance compared to all other GDL samples; however, it exhibits a fairly low *in-plane* resistance. Although Tenax woven samples have shown comparable values to those obtained for paper GDLs. These values obtained fall within the range reported by Mishra *et al.* [45] and Zhang *et al.* [46].

For the *in-plane* resistance measurements, the resistance (R) was measured at various locations along the GDL strip samples yielding a straight line (Fig. 22), the slope of which represents the resistance per unit distance. The resistivity (in Ω m) of the GDL was then calculated using Ohm's Law as shown in Equations (1) and (2). Here, it can be noticed that the plot does not go through the origin (0,0) which is mainly due to the contact resistance between the GDL and measurement rods.

The results of the *in-plane* resistivity experiments (Fig. 23) show low values for the woven GDLs, which can be explained by the uniform interconnection between the fibres allowing electrons to
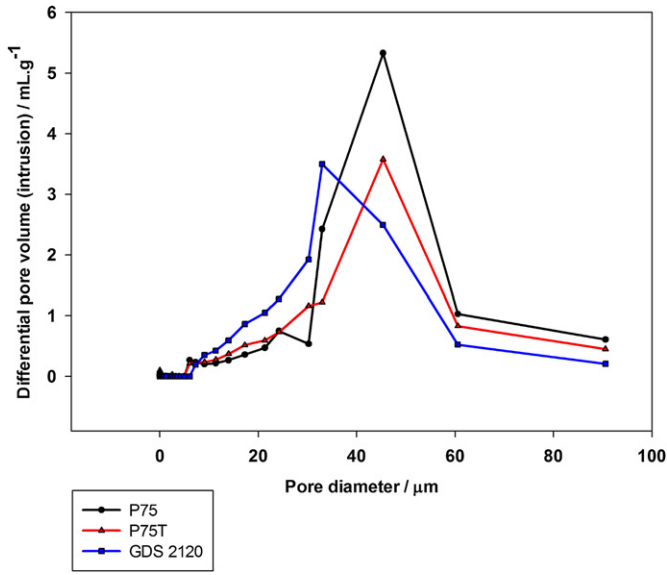
Fig. 15. Pore size distribution change between unteflonated, teflonated and teflonated with a MPL GDL samples.
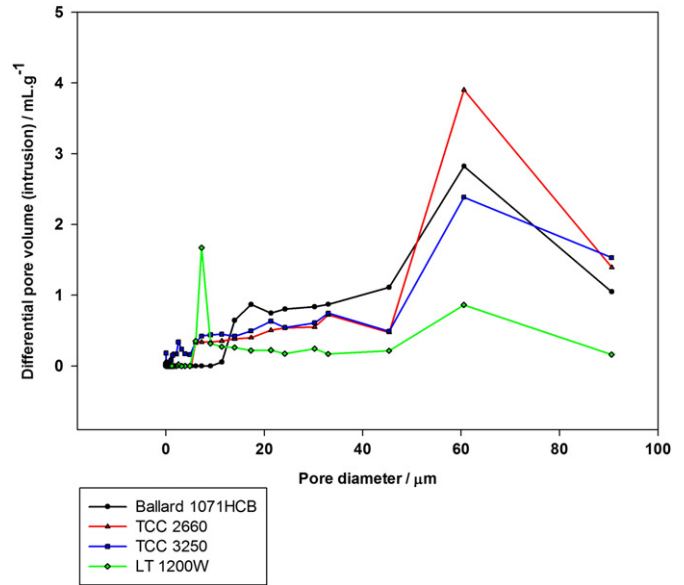

Fig. 17. Pore size distribution for commercial woven GDL.

flow through the GDL 'easily'. In the same manner, felt fibre GDL papers exhibit lower *in-plane* resistivity values due to the ability of the electrons to travel through the three dimensional configuration through fibres crossing different layers, rather than, the layered webs that are interconnected on contact points at each layer.

A trend in the *in-plane* resistance can be observed (Fig. 23) for the Sigracet P50 and P70 substrates group. For example, the resistance decreases with PTFE loading but also increases in the presence of MPL. This interesting finding suggests that possibly some of the MPL penetrates through the substrate, in turn covering some fibres and hence insulating them due to the presence of PTFE and therefore increasing the resistivity. However the reason for the decrease in resistivity with PTFE loading is not clear. It can be suggested that the PTFE works as a binder when applied and enhances the 'contact' between the fibres in the GDL. A similar

finding was observed by Ismail *et al.* [47] when increasing PTFE loading in the MPL. Several possible explanations were made by the authors to elucidate this finding however the explanations were not backed up by clear experimental results.

In-plane resistivity values for Toray shows the lowest resistivity for GDL papers. This could be due to high graphitisation level of the GDL fibres which enhances the electrical conductance of the substrate. It is also shown that the GDL resistivity decreases with GDL thickness which can be explained by the increase of the bulk density of the GDL. This observation suggests that higher fibre density provides a larger bulk for electron transfer. On the other hand, the *in-plane* resistivity values of C4 and C8 are higher than those of C2 and C6. Knowing the fact that C2 and C4 are based on the same substrate and similarly for C6 and C8, this finding suggests that the increase in resistivity is directly related to the MPL properties. The resistivity values are in agreement with the values reported by Williams *et al.* [11].
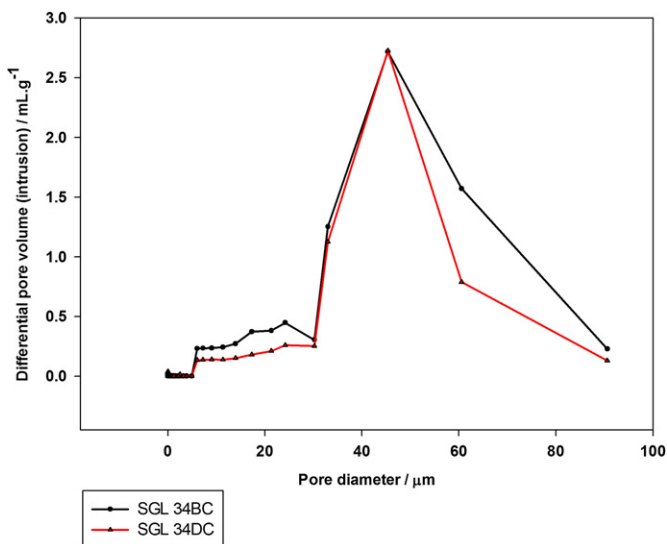

Fig. 16. GDL pore size distribution change due to the increase of PTFE loading in the sample.
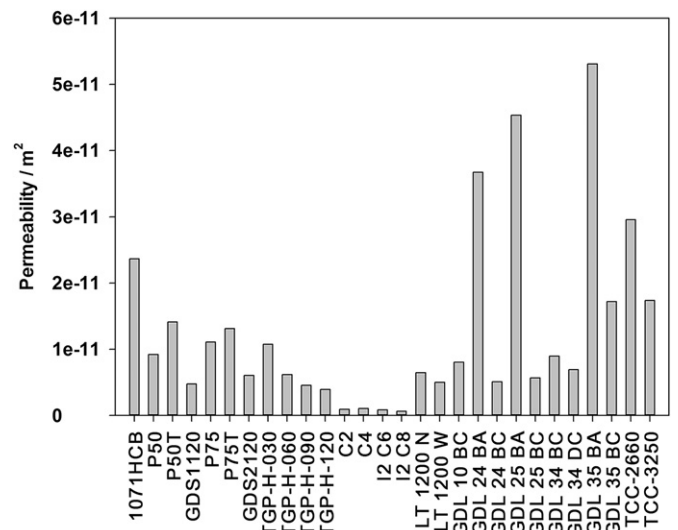

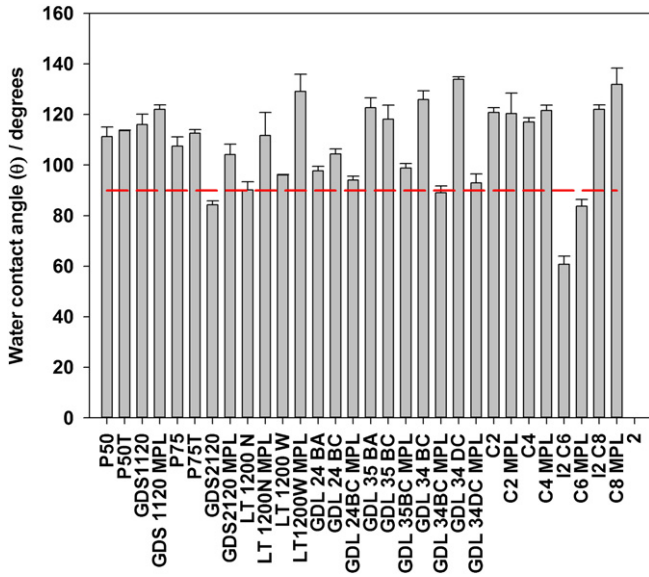**Fig. 18.** GDL permeability as measured using mercury porosimeter.

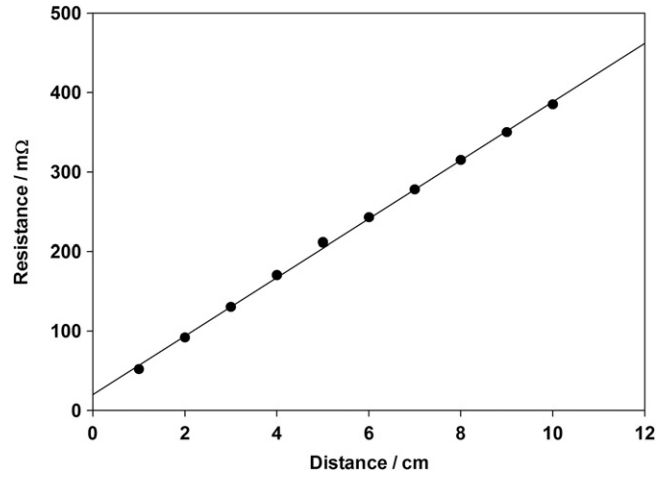**Fig. 19.** Water contact angle for commercial GDLs and their MPLs.

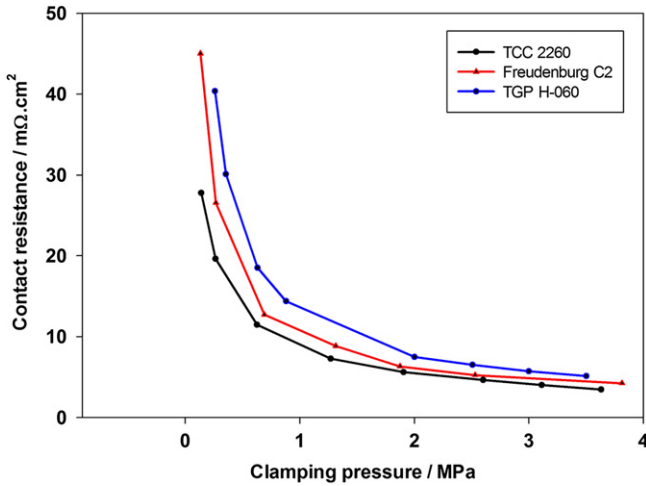**Fig. 22.** Toray H-030 strip resistance change with distance.

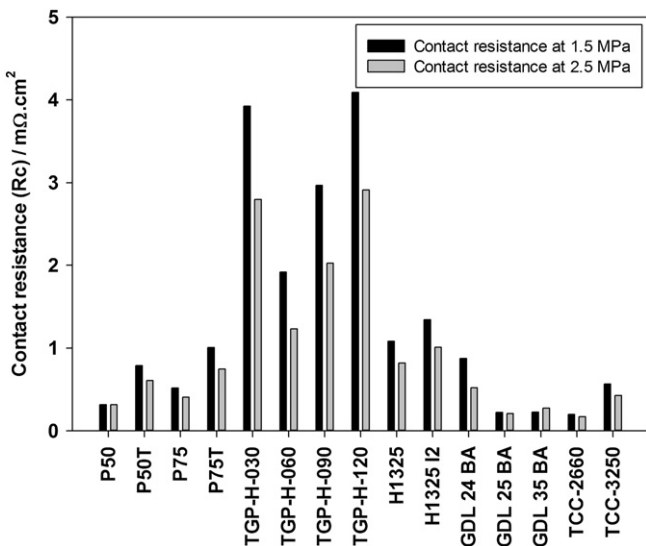**Fig. 20.** Contact resistance change with clamping pressure.

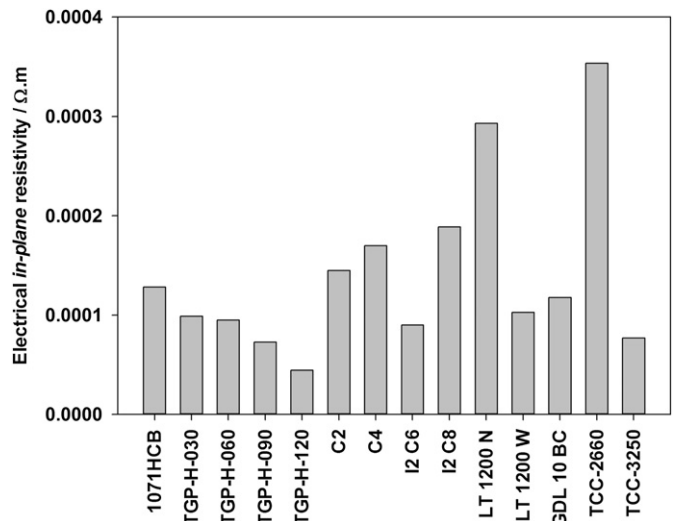**Fig. 23.** *In-plane* resistivity of various GDL materials.

Fig. 21. Commercial GDL contact resistance with POCO AXF-5Q graphite plate at 1.5 and 2.5 MPa.

4. Conclusions

In this technical paper, the data of important *ex-situ* parameters of commercial GDLs used in PEM fuel cells are reported. The results indicate that there is a relationship between the GDL properties, substrate structure, PTFE and MPL loading. It was found that PTFE loading in the GDL decreases porosity and resistivity; however, it increases tortuosity, permeability and hydrophobicity. Adding an MPL to the GDL results in a further decrease in porosity and permeability and increase in tortuosity and resistivity. Furthermore, different MPL structures were observed and the variations on their effect on the surface roughness and hydrophobicity were investigated. It was also shown that the contact resistance between the GDL and the POCO flow field plate increases with thickness and PTFE loading. This study also shows the need for further research to explore the effect of PTFE on the GDL and to assist in explaining the changes in its other properties. Moreover, novel methods for measuring GDL characteristics/properties are required to eliminate errors due to the assumptions made in designing testing setup.

This paper offers values and parameters for a wide range of GDL properties that are required for PEM fuel cell designers and modellers. This study will extend further to cover other crucial GDL characteristics, namely, material composition and *through-plane* and *in-plane* permeability for water, hydrogen, oxygen and air. The complete study of *ex-situ* characterisation of GDLs coupled with GDL modelling and *in-situ* testing will assist GDL manufacturers in developing GDLs with higher performance for the various fuel cell applications, and will lead to the development of GDL selection criteria for PEM fuel cells.

Acknowledgements

References

[1] S. Litster, G. McLean, Journal of Power Sources 130 (1–2) (2004) 61–76.
[2] H. Li, et al., Journal of Power Sources 178 (1) (2008) 103–117.
[3] J.P. Owejan, et al., Effects of Flow Field and Diffusion Layer Properties on Water Accumulation in a Pem Fuel Cell. Icnmm2007: Proceedings of the 5th International Conference on Nanochannels, Microchannels, and Minichannels, Amer. Soc. Mechanical Engineers, New York, 2007, pp. 311–320.
[4] C. Lim, C.Y. Wang, Electrochimica Acta 49 (24) (2004) 4149–4156.
[5] S. Kundu, et al., Journal of Power Sources 179 (2) (2008) 693–699.
[6] J.-H. Lin, et al., Energy & Fuels 22 (4) (2008) 2533–2538.
[7] A. El-kharouf, B.G. Pollet, Chapter 4-Gas Diffusion Media and Their Degradation, in Polymer Electrolyte Fuel Cell Degradation, Academic Press, Boston, 2012, pp. 215–247.
[8] L. Cindrella, et al., Journal of Power Sources 194 (1) (2009) 146–160.
[9] J.P. Feser, A.K. Prasad, S.G. Advani, Journal of Power Sources 162 (2) (2006) 1226–1231.
[10] A. Tamayol, M. Bahrami, Journal of Power Sources 196 (15) (2011) 6356–6361.
[11] M.V. Williams, et al., Journal of the Electrochemical Society 151 (8) (2004) A1173–A1180.
[12] G.-G. Park, et al., Journal of Power Sources 131 (1–2) (2004) 182–187.
[13] S. Park, J.-W. Lee, B.N. Popov, Journal of Power Sources 163 (1) (2006) 357–363.
[14] B. Millington, S. Du, B.G. Pollet, Journal of Power Sources 196 (21) (2011) 9013–9017.
[15] M. Prasanna, et al., Journal of Power Sources 131 (1–2) (2004) 147–154.
[16] C. Lee, W. Mérida, Journal of Power Sources 164 (1) (2007) 141–153.
[17] R. John Felix Kumar, V. Radhakrishnan, P. Haridoss, Effect of electrochemical aging on the interaction between gas diffusion layers and the flow field in a proton exchange membrane fuel cell, International Journal of Hydrogen Energy 36 (12) (2011) 7207–7211.
[18] J.A. Paleaz, S.G. Kandlikar, Effects of Freezing and Thawing on the Structures of Porous Gas Diffusion Media in the Fifth International Conference on Nanochannels, Microchannels and Minichannels, 2007 (Puebla, Mexico).
[19] V. Radhakrishnan, P. Haridoss, International Journal of Hydrogen Energy 35 (20) (2010) 11107–11118.
[20] J. Scholta, K. Seidenberger and F. Wilhelm, Gas Diffusion Layer (GDL) degradation in polymer electrolyte fuel cells, in: 2nd CARISMA international conference on progress in MEA materials fro medium and high temperature polymer electrolytes fuel cells, 2010.
[21] W.-k. Lee, et al., Journal of Power Sources 84 (1) (1999) 45–51.
[22] J. Ge, A. Higier, H. Liu, Journal of Power Sources 159 (2) (2006) 922–927.
[23] X.Q. Xing, et al., Journal of Power Sources 195 (1) (2010) 62–68.
[24] S.G. Kandlikar, et al., Journal of Power Sources 194 (1) (2009) 328–337.
[25] Y.-H. Lai, et al., Journal of Power Sources 184 (1) (2008) 120–128.
[26] J.T. Gostick, et al., Journal of Power Sources 162 (1) (2006) 228–238.
[27] T. Zhou, H. Liu, Journal of Power Sources 161 (1) (2006) 444–453.
[28] H. Meng, C.-Y. Wang, Journal of the Electrochemical Society 151 (3) (2004) A358–A367.
[29] H. Sun, et al., Journal of Power Sources 158 (1) (2006) 326–332.
[30] M. Noponen, et al., Journal of Power Sources 106 (1–2) (2002) 304–312.
[31] M.M. Mench, C.Y. Wang, M. Ishikawa, Journal of the Electrochemical Society 150 (8) (2003) A1052–A1059.
[32] G. Karimi, X. Li, P. Teertstra, Electrochimica Acta 55 (5) (2010) 1619–1625.
[33] E. Sadeghi, N. Djilali, M. Bahrami, Journal of Power Sources 195 (24) (2010) 8104–8109.
[34] P.A. Webb, An Introduction to the Physical Characterization of Materials by Mercury Intrusion Porosimetry with Emphasis on Reduction and Presentation of Experimental Data, Micromeritics Instrument Corp., Norcross, Georgia, 2001.
[35] X.L. Wang, et al., Electrochimica Acta 51 (23) (2006) 4909–4915.
[36] MatWeb_LCC. POCO Graphite AXF-5Q Specialty Graphite. Available from: http://www.matweb.com/search/datasheet.aspx? matguid=71a29c978b28410b8e392076be858c76&ckck=1.
[37] W.R. Chang, et al., Journal of Power Sources 166 (1) (2007) 149–154.
[38] P.M. Wilde, et al., Fuel Cells 4 (3) (2004) 180–184.
[39] P.J. Rae, D.M. Dattelbaum, Polymer 45 (22) (2004) 7615–7625.
[40] B. Avasarala, P. Haldar, Journal of Power Sources 188 (1) (2009) 225–229.
[41] M.M. Mench, Fuel Cell Engines, John Wiley & Sons, Inc., 2008.
[42] Z. Fishman, A. Bazylak, Journal of the Electrochemical Society 158 (2) (2011) B247–B252.
[43] E.-D. Wang, P.-F. Shi, C.-Y. Du, Electrochemistry Communications 10 (4) (2008) 555–558.
[44] J. Benziger, et al., Journal of Membrane Science 261 (1–2) (2005) 98–106.
[45] V. Mishra, F. Yang, R. Pitchumani, Journal of Fuel Cell Science and Technology 1 (1) (2004) 2–9.
[46] L. Zhang, et al., Journal of Power Sources 162 (2) (2006) 1165–1171.
[47] M.S. Ismail, et al., Journal of Power Sources 195 (9) (2010) 2700–2708.